

Alkali-activated materials for radionuclide immobilisation and the effect of precursor composition on Cs/Sr retention

Peer-reviewed author version

VANDEVENNE, Niels; Ion Iacobescu, Remus; CARLEER, Robert; SAMYN, Pieter; D'HAEN, Jan; Pontikes, Yiannis; SCHREURS, Sonja & SCHROEYERS, Wouter (2018) Alkali-activated materials for radionuclide immobilisation and the effect of precursor composition on Cs/Sr retention. In: JOURNAL OF NUCLEAR MATERIALS, 510, p. 575-584.

DOI: 10.1016/j.jnucmat.2018.08.045

Handle: <http://hdl.handle.net/1942/26732>

1 **Alkali-activated materials for radionuclide immobilisation and the**  
2 **effect of precursor composition on Cs/Sr retention**

3 Niels Vandevenne <sup>a</sup>, Remus Ion Iacobescu <sup>b</sup>, Robert Carleer <sup>c</sup>, Pieter Samyn <sup>c</sup>, Jan D'Haen<sup>d,e</sup>, Yiannis Pontikes <sup>b</sup>,  
4 Sonja Schreurs <sup>a</sup>, Wouter Schroeyers <sup>a,\*</sup>

5 <sup>a</sup> Hasselt University, CMK, Nuclear Technological Centre, Agoralaan, Gebouw H, 3590 Diepenbeek, Belgium

6 <sup>b</sup> KU Leuven, Department of Materials Engineering, Kasteelpark Arenberg 44, 3001 Leuven, Belgium

7 <sup>c</sup> Hasselt University, CMK, Research Group of Applied and Analytical Chemistry, Agoralaan, Gebouw D, 3590  
8 Diepenbeek, Belgium

9 <sup>d</sup> Hasselt University, Institute for Materials Research (IMO), Wetenschapspark 1, 3590 Diepenbeek, Belgium

10 <sup>e</sup> IMEC, Division IMOMECE, Wetenschapspark 1, 3590 Diepenbeek, Belgium

11  
12  
13  
14 \* Corresponding author: Prof. Dr. Wouter Schroeyers, e-mail address:

15 wouter.schroeyers@uhasselt.be  
16  
17

## 18 **Abstract**

19 One of the major challenges for the nuclear industry is the safe and sustainable immobilisation of  
20 radioactive wastes (RAW). Currently, the most commonly used immobilisation matrices for low and  
21 intermediate level wastes are based on ordinary Portland cement. For the more difficult to  
22 immobilise nuclides, such as caesium ( $\text{Cs}^+$ ) and strontium ( $\text{Sr}^{2+}$ ), researchers have been studying  
23 alternative immobilisation matrices, of which alkali-activated materials (AAM) are a very promising  
24 option. However, the differences in precursor compositions and the use of different types of  
25 activating solutions make it difficult to fully understand the effects of precursor composition on the  
26 immobilisation of introduced nuclides. Therefore, six different compositions of laboratory-  
27 synthesized Ca-Si-Al slags were developed to serve as precursors for low-alkaline AAMs to study their  
28 immobilisation behaviour. Immobilisation capacities up to 97.6 %  $\text{Cs}^+$  and 99.9 %  $\text{Sr}^{2+}$  were achieved  
29 with 1 wt% waste loading when leaching for 7 days at 20 °C in Milli Q water.  $\text{Cs}^+$  immobilisation is  
30 higher at lower Si/Al and Ca/(Si+Al) ratios. Immobilisation of  $\text{Sr}^{2+}$  is higher at a lower Ca/(Si+Al) ratio  
31 and independent of Si/Al ratio. The results of this study offer a deeper understanding of the  
32 immobilisation behaviour of AAMs and can encourage further research and application of AAMs for  
33 RAW immobilisation.

## 34 **Keywords**

35 **Alkali-activated material; immobilisation; radioactive waste; caesium; strontium**

## 36 **1 Introduction**

37 In the pursuit of a sustainable society, one of the main challenges for researchers and industries is  
38 the safe management and disposal of industrial wastes, with radioactive waste (RAW) being  
39 particularly important. RAW is produced by many different sources; the main ones being the energy  
40 sector (nuclear fuel cycle), the dismantling of nuclear installations, and applications in medicine,

41 agriculture and industry. Because of the ever-increasing amounts of RAW, continuous innovation in  
42 immobilisation is becoming more and more important. As an alternative to the currently widely used  
43 cementitious immobilisation matrices, alkali-activated materials (AAM) have been increasingly  
44 studied. Depending on the type of precursor and the composition of the hydration products, AAMs  
45 (or subclasses thereof) are also known as geopolymers, inorganic polymers, soil cements,  
46 geocements, alkaline cements, zeoceramics, alkali-activated slag cement and a variety of other  
47 names [1,2]. AAMs have demonstrated promising results in immobilising radionuclides such as  
48 caesium and strontium [3-22]. As an example, the superior Cs<sup>+</sup> retention of AAMs was reported by  
49 *Shi and Fernández-Jiménez* (2006) [9], who tested leaching of Cs<sup>+</sup> and Sr<sup>2+</sup> from AAMs containing  
50 zeolites and/or metakaolin (MK) as additives. They concluded that wastes show much less  
51 interference with the hydration of AAMs than that of ordinary Portland cement. *Blackford et al.*  
52 (2007) [11] developed a geopolymer matrix derived from MK, in which Cs<sup>+</sup> was introduced. They  
53 concluded that Cs<sup>+</sup> was fully incorporated into the amorphous geopolymer phase, proving the  
54 potential of AAMs for RAW immobilisation. In addition to the immobilisation of Cs<sup>+</sup> and Sr<sup>2+</sup>, other  
55 elements such as Cd<sup>2+</sup> and Pb<sup>2+</sup> [23], and radionuclides such as <sup>152</sup>Eu, <sup>60</sup>Co, <sup>59</sup>Fe and isotopes of Am  
56 and Pu have also been successfully immobilised in AAMs [24–26].

57 Concerning the use of AAMs for RAW immobilisation, most literature covers AAMs based on  
58 commercial recipes, MK, fly ash (FA), ground granulated blast furnace slag (GGBFS) or combinations  
59 thereof. Despite the large body of research and the promising immobilisation results, a systematic  
60 study of the influence of the precursor composition on the immobilisation capacities for Cs<sup>+</sup> and Sr<sup>2+</sup>  
61 is lacking. According to *Aly et al.* (2008) [12], MK-based AAMs show optimal leach resistance at Si/Al  
62 ratios higher than 2. They reported a sharp decrease in the Cs<sup>+</sup> release when the Si/Al ratio increased  
63 from 1.5 to 2 followed by a gradual increase at Si/Al ratios higher than 3, reaching the lowest value at  
64 Si/Al ratio of 2. For Sr<sup>2+</sup>, the lowest release was obtained at a Si/Al ratio of 1.5, increasing gradually  
65 with increasing Si/Al ratio [12].

66 Almost all concerning literature describes AAMs made from industrial residues, making it difficult to  
67 exclude effects of trace elements in the precursor on the immobilisation capacities. Also, the variety  
68 in precursor origin and composition in most studies make it difficult to generalize the drawn  
69 conclusions, since the immobilisation performance is very dependent on the design parameters. In  
70 addition, there exists a wide variety of alkali-activators used, most often consisting of highly-alkaline  
71 activating solutions and often containing sodium silicates.

72 According to the IAEA [27], the lack of standards for precursors, experience of process optimization,  
73 and demonstration of long-term stability limit their use in RAW immobilisation, despite the reported  
74 favourable experiences using AAMs. They stated that novel materials need a better benchmarking,  
75 and emphasised that it is also important to realise that existing test methods do not always give  
76 comparable results with different classes of materials [27]. Therefore, the effect of precursor  
77 composition on the immobilisation of  $\text{Cs}^+$  and  $\text{Sr}^{2+}$  in AAMs is studied in this work, by developing  
78 synthetic Ca-Si-Al slag precursors with different compositions from laboratory reagents, yielding Si/Al  
79 and Ca/(Si+Al) molar ratios of 0.95 – 5.1 and 0.42 – 1.0 respectively. In this way, immobilisation is  
80 studied excluding possible effects of trace elements in the mixture. The present results can be  
81 further used as a guideline for choosing industrial residues with a proper composition or for using  
82 proper mixing ratios.

## 83 **2 Materials and methods**

### 84 *2.1 Ca-Si-Al slag synthesis*

85 Ca-Si-Al slags were synthesised from analytical grade laboratory reagents  $\text{Al}_2\text{O}_3$ ,  $\text{SiO}_2$  and  $\text{CaCO}_3$  (all  
86 Sigma-Aldrich, > 99 % pure). The studied compositions (**Table 1**) were chosen to broadly resemble  
87 GGBFS and to be fully liquid at 1550 °C (see **Figure 1**). The  $\text{CaCO}_3$  was first calcined in a muffle  
88 furnace at 1050 °C overnight to expel  $\text{CO}_2$ . For each composition, the exact mass of  $\text{CaCO}_3$  necessary  
89 for achieving the stoichiometric amount of CaO was weighed and inserted into the muffle furnace.

90 Immediately after cooling, the mass of the obtained CaO was determined to verify the complete  
 91 decarbonation. The resulting CaO was then mixed with weighed amounts of Al<sub>2</sub>O<sub>3</sub> and SiO<sub>2</sub> for two  
 92 hours in a Turbula T2C mixer for homogenization. The mixtures were placed in a platinum crucible  
 93 and inserted into a bottom loading furnace (AGNI ELT 160-02) at 1630 °C. A higher temperature was  
 94 applied to account for possible differences in temperature between the location of the crucible and  
 95 the thermocouple of the furnace, to ensure that the sample would melt completely. After an  
 96 isothermal period of 2.5 h, the melt was quenched by pouring in water at room temperature. The  
 97 cooled slag was then dried at 110 °C to constant weight before being crushed and milled in a Retsch  
 98 disk mill RS200 at 1000 rpm for 60 s.

99 Homogeneity of the finely milled slag was confirmed by X-ray diffraction spectroscopy (XRD). The  
 100 measurements were performed with a Bruker D8 diffractometer. This theta-theta diffractometer is  
 101 equipped with a Göbel mirror (line focus, Cu k<sub>α</sub> radiation). The X-rays are detected with a 1D lynxeye  
 102 detector.

103 The specific surface area of the resulting powders was measured in threefold by use of Blaine  
 104 method. The procedures described in the standard EN 196-6 [28] were followed as closely as possible  
 105 and the measurements were performed against a reference cement sample. It is, however,  
 106 important to note that the Blaine method is designed for cements and that results may deviate when  
 107 using other types of materials.

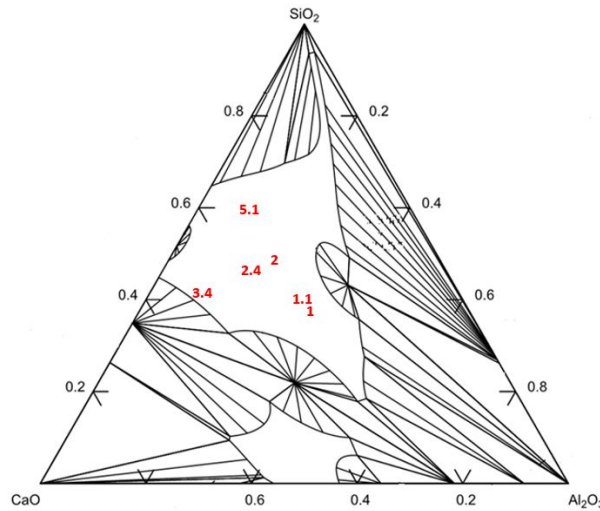
108 **Table 1:** Designed compositions of synthetic slags (wt fraction) and the initial Si/Al and Ca/(Si+Al)  
 109 molar ratios. The labelling of the samples is based on the initial Si/Al ratio.

	SiO <sub>2</sub>	Al <sub>2</sub> O <sub>3</sub>	CaO	Si/Al	Ca/(Si+Al)
	<i>wt fraction</i>	<i>wt fraction</i>	<i>wt fraction</i>	<i>mol/mol</i>	<i>mol/mol</i>
S_1	0.37	0.33	0.30	0.95	0.42
S_1.1	0.40	0.30	0.30	1.1	0.43
S_2	0.49	0.21	0.30	2.0	0.44
S_2.4	0.47	0.17	0.36	2.4	0.59

S_3.4	0.40	0.10	0.50	3.4	1.0
S_3.4b*	0.40	0.10	0.50	3.4	1.0
S_5.1	0.60	0.10	0.30	5.1	0.45

\*This composition, randomly chosen, has been made as a replicate to check the reproducibility of the experimental design

110



111

112 **Figure 1:** Phase diagram at 1550 °C. The designed compositions are all within the liquid (white) area.

113 2.2 AAM elaboration

114 AAM pastes were prepared by mixing the powdered slag precursors with a 2 M NaOH solution  
115 (prepared from NaOH pellets (Fischer Scientific, 98.44 % pure) and type II distilled water) using a  
116 laboratory mixer and maintaining a liquid to solid ratio (L/S) of 0.30. These parameters were chosen  
117 based on our earlier study [29] and adjusted for optimal workability and setting time. At this molarity  
118 and L/S ratio, the amount of Na<sup>+</sup> added is 1 wt% for each sample. Cs<sup>+</sup> and Sr<sup>2+</sup> were added as nitrates  
119 (CsNO<sub>3</sub>, Alfa Aesar 99.8%; Sr(NO<sub>3</sub>)<sub>2</sub>, Emsure 99.0%) to account for 1 wt% and 0.1 wt% respectively of  
120 the final AAM-mass (solid precursor + activating solution). A lower wt% of Sr<sup>2+</sup> was chosen to avoid  
121 significant interference with the polymerisation kinetics, as reported in our earlier studies [29,30].  
122 The resulting mixtures were poured into plastic (polymethylmethacrylate, PMMA) 25 x 25 x 20 mm<sup>3</sup>  
123 moulds. The moulds were manually tapped during 60 seconds to remove air bubbles before being

124 sealed with a PMMA cap. These pastes were then allowed to cure for 28 days at  $23 \pm 1$  °C. Each  
125 composition was made in threefold for the leaching experiments.

### 126 2.3 Leaching of introduced and structural elements

127 The release of introduced caesium and strontium, and of the structural elements silicon, aluminium,  
128 calcium and sodium was measured using a semi-dynamic diffusion test described in our earlier study  
129 [29] and based on the standards ASTM C1220-98 [31] and CEN/TS 15863:2015 [32]. The samples  
130 were demoulded, cleaned with a dry brush and measured for dimensions and weight before being  
131 submerged in 400 ml of pre-heated Milli-Q water (90 °C, polypropylene bottle and sample holder).  
132 Before and after the eluate was refreshed, the mass of the closed container was measured to  
133 determine water loss through evaporation. In all cases, the loss of mass through evaporation was  
134 lower than 2 %, which is in line with the standard ASTM C1220-98 [31]. At each sampling time (1 h,  
135 24 h, 7 d, 28 d), 10.0 ml of the eluate was filtered over a 0.2 µm syringe filter and acidified  
136 immediately after sampling to a concentration of 2 % HNO<sub>3</sub> (MERCK Suprapur 65 %). The  
137 concentrations of water-soluble Sr<sup>2+</sup>, Si<sup>4+</sup>, Al<sup>3+</sup>, Ca<sup>2+</sup>, and Na<sup>+</sup> were measured by ICP-OES (Perkin Elmer  
138 type Optima 8300) in axial mode. The concentration of water-soluble Cs<sup>+</sup> was measured by ICP-MS  
139 (Perkin Elmer NexION 350S). At each sampling time, the eluate was also measured for pH (calibrated  
140 electrode HI1043B, Hanna Instruments) and conductivity (Schott Geräte CG 858, calibrated with 0.1  
141 M KCl).

142 The release  $r$  (mg/m<sup>2</sup>) of element  $i$  at leaching interval  $n$  is calculated as:

$$r_{i,n} = \frac{(C_{i,n} - B_{i,n}) \cdot V}{A_s} \quad (1)$$

143 With

144  $C_{i,n}$  = concentration of element  $i$  in the filtered aliquot of leaching interval  $n$  (mg/ml)

145  $B_{i,n}$  = concentration of element  $i$  in the filtered blanc aliquot of leaching interval  $n$  (mg/ml)



146  $V$  = initial volume of eluate in the bottle containing the sample AAM (ml)

147  $A_s$  = geometric surface area of the sample AAM (m<sup>2</sup>)

148 The cumulative release  $R$  (mg/m<sup>2</sup>) of each constituent is calculated as:

$$R_i = \sum_0^n r_{i,n} \quad (2)$$

149 The normalized leach rate  $LR$  (mg/(m<sup>2</sup>.s)) of element  $i$  at leaching interval  $n$  is calculated as:

$$LR_{i,n} = \frac{r_{i,n}}{\Delta t_n \cdot f_i} \quad (3)$$

150 with  $\Delta t_n$  the time of leaching interval  $n$  (in seconds) and  $f_i$  the fraction of element  $i$  in the sample, as

151 to account for possible differences in waste loadings. The total release of element  $i$  ( $\% release_i$ ) and

152 the percentage of wash-off in the first leaching interval ( $\% WO_i$ ) are defined as:

$$\% release_i = \frac{R_{i,28d} \cdot A_s}{m_s \cdot f_i} \cdot 100 \% \quad (4)$$

$$\% WO_i = \frac{R_{i,1h}}{R_{i,28d}} \cdot 100 \% \quad (5)$$

153 with  $m_s$  the mass of the sample (mg) after demoulding.

#### 154 2.4 Effect of leaching temperature and specific surface area on immobilisation performance

155 To confirm the observed relation between immobilisation capacity and the AAM design ratios, the

156 immobilisation capacity of selected compositions has been tested under varying conditions. Samples

157 of compositions AAM\_1, AAM\_1.1, AAM\_2 and AAM\_5.1 were leached at a lower temperature of 20

158  $\pm 1$  °C for 7 days. The specific surface area of these samples was measured. The Brunauer Emmett

159 Teller (BET) surface area, was measured for these samples by continuous flow method using 0.3

160 ml/min of nitrogen gas (Tristar 3000).

161 2.5 *Effect of slag fineness on immobilisation performance*

162 The effect of slag fineness on the immobilisation performance is studied by further milling slag

163 precursors S\_1 and S\_2 for an additional 30 s. From these finer slags, additional samples of

164 composition AAM\_1 and AAM\_2 were prepared for leaching during 7 d at  $20 \pm 1$  °C.

165

166 **3 Results and discussion**

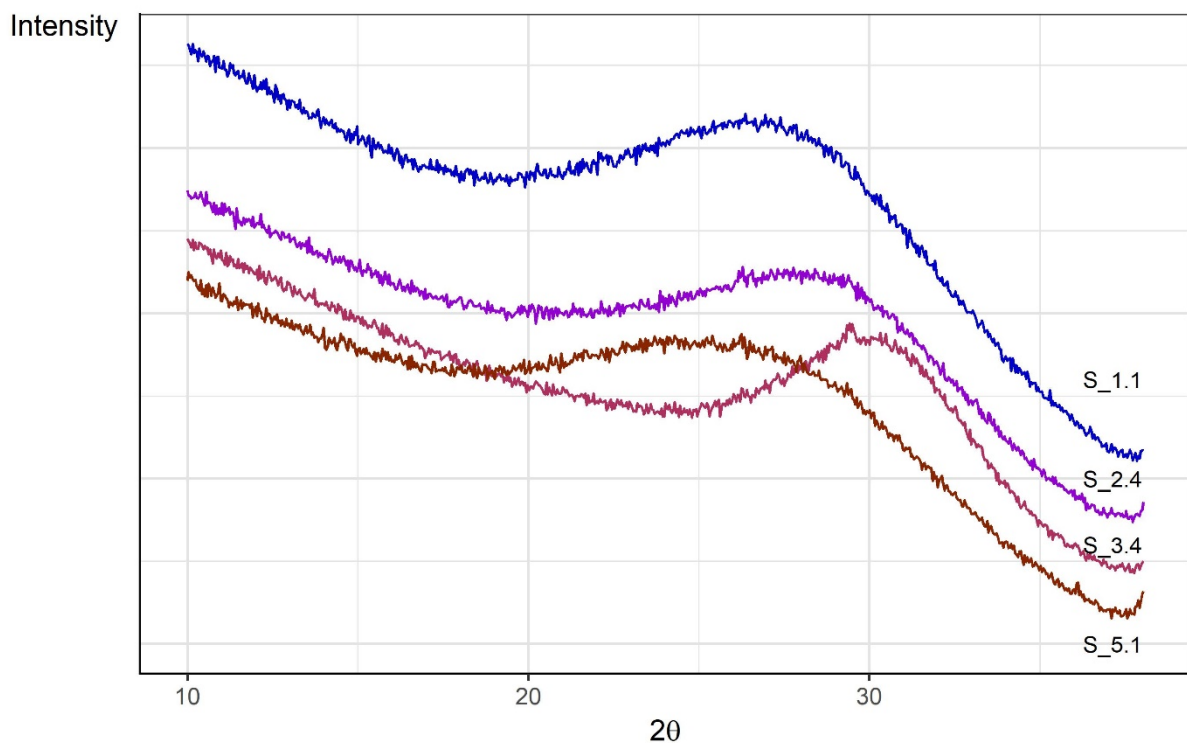
167 3.1 *Homogeneity of the slag*

168 All mixtures were completely molten during the isothermal period in the bottom loading furnace.

169 Water-quenching of the melt gave rise to a clear transparent glass for all mixtures. XRD patterns of

170 selected slag samples S\_1.1, S\_2.4, S\_3.4 and S\_5.1 are presented in **Figure 2**. No crystalline phases

171 were detected in any of the measured slags, indicating homogeneity without crystalline inclusions.



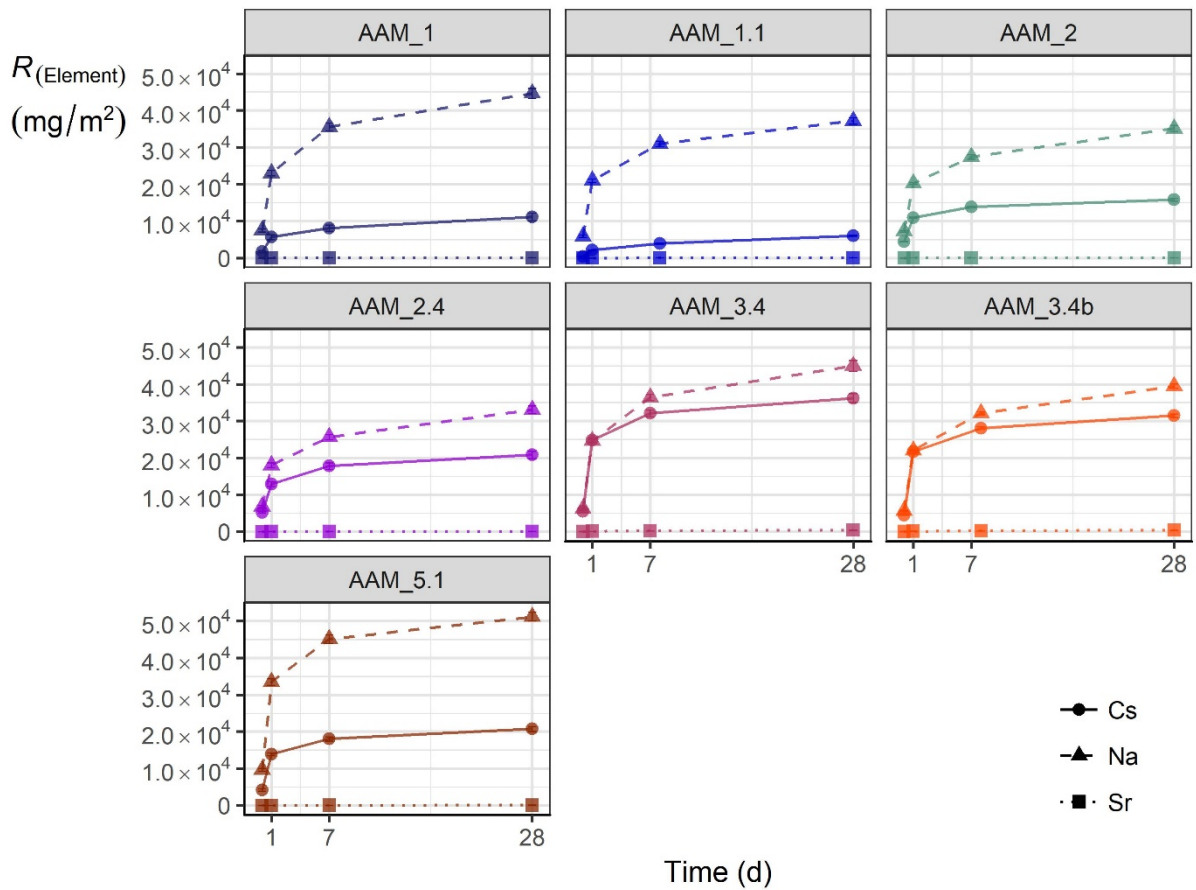
172

173 **Figure 2:** XRD patterns of the finely milled slags S\_1.1, S\_2.4, S\_3.4 and S\_5.1.

174 3.2 Immobilisation of  $\text{Cs}^+$ ,  $\text{Sr}^{2+}$  and  $\text{Na}^+$

175 **Figure 3** shows the cumulative release for  $\text{Cs}^+$ ,  $\text{Sr}^{2+}$  and  $\text{Na}^+$  in function of the leaching time. The  
176 % release is summarized in **Table 2**. The highest  $\text{Na}^+$  leaching is measured in AAM\_5.1, which is also  
177 the sample with the highest Si/Al ratio. AAM\_1.1 shows the best  $\text{Cs}^+$  immobilisation, releasing only  
178  $7.8 \pm 0.3$  % of the introduced  $\text{Cs}^+$ , which is almost twice as good as the second best (AAM\_1). In our  
179 earlier study [29], GGBFS-based AAMs activated with 6 M NaOH were leached for 7 days under the  
180 same conditions. The composition of the GGBFS closely resembles that of S\_3.4 (excluding the  
181 contribution of MgO,  $\text{SO}_3$  and other trace elements). With a 1 wt%  $\text{Cs}^+$  loading, the GGBFS-AAM  
182 leached 66 % of the introduced  $\text{Cs}^+$  [29]. This is much higher than the  $\text{Cs}^+$  release observed in  
183 AAM\_3.4 and AAM\_3.4b which could be due to e.g. the differences in activating solution molarity or  
184 the presence of magnesium and other elements. Among the compositions tested in this study,  
185 AAM\_3.4 performs worst regarding both  $\text{Cs}^+$  and  $\text{Sr}^{2+}$  immobilisation indicating that the composition  
186 of GGBFS requires optimisation regarding immobilisation purposes.

187 The  $\text{Cs}^+$  and  $\text{Sr}^{2+}$  normalized leach rates are given in **Table 3**. The effect of initial wash-off ( $\%WO_{\text{Cs}}$ )  
188 seems to be the least pronounced for AAM\_1.1 (see **Table 3**) with a percentage released in the first  
189 hour of leaching of 7 % of the total amount leached. Also for  $\text{Sr}^{2+}$ , AAM\_1.1 clearly shows the best  
190 immobilisation, releasing only  $0.50 \pm 0.04$  % of the introduced  $\text{Sr}^{2+}$ , which is about 50 % better than  
191 the second best (AAM\_2). The overall percentage of wash-off ( $\%WO_{\text{Sr}}$ , see **Table 3**) is lower for  $\text{Sr}^{2+}$   
192 than for  $\text{Cs}^+$  indicating a slower release from the sample surface.



193

194

**Figure 3:** Cumulative release of  $\text{Cs}^+$ ,  $\text{Na}^+$  and  $\text{Sr}^{2+}$  during a 28-d leaching test at 90 °C.

195

**Table 2:** Percentage of introduced  $\text{Cs}^+$ ,  $\text{Sr}^{2+}$  and  $\text{Na}^+$  that has been released by leaching for 28 d at 90

196

°C. Uncertainties are calculated as standard deviations from 3 samples per composition.

$\% \text{ release}_i$	$\text{Cs}^+$	$\text{Sr}^{2+}$	$\text{Na}^+$
AAM_1	14 ± 2	1.11 ± 0.07	58 ± 2
AAM_1.1	7.8 ± 0.3	0.5 ± 0.04	49 ± 2
AAM_2	20.1 ± 0.5	0.74 ± 0.3	46 ± 1
AAM_2.4	40 ± 2	1.4 ± 0.2	65 ± 2
AAM_3.4	46 ± 2	4.9 ± 0.5	59 ± 2
AAM_3.4b	40.9 ± 0.7	5 ± 0.4	53 ± 1
AAM_5.1	27.8 ± 0.9	0.9 ± 0.1	71 ± 2

197

198 **Table 3:** Average leach rates (mg/(m<sup>2</sup>.s)) of Cs<sup>+</sup> and Sr<sup>2+</sup> during a 28-d leaching period at 90 °C. The  
 199 mean value calculated per sample is weighted for the time of the respective leaching interval. %WO<sub>i</sub>  
 200 (wash-off) is the percentage of the total released amount leached in the first hour of the test.

	Leaching time (h)	AAM_1	AAM_1.1*	AAM_2	AAM_2.4	AAM_3.4	AAM_3.4b*	AAM_5.1
<i>LR<sub>Cs</sub></i>	1	49	12	120	150	150	120	120
	24	4.7	2.0	7.8	9.3	23	21	12
	168/ 192*	0.47	0.30	0.55	0.94	1.4	1.1	0.80
	672	0.13	0.09	0.09	0.13	0.18	0.14	0.12
<i>Mean</i>		0.43	0.23	0.64	0.83	1.5	1.3	0.83
<i>%WO<sub>Cs</sub></i>		16	7	28	25	15	14	20
<i>LR<sub>Sr</sub></i>	1	0.68	0.53	0.39	1.5	10	12	0.77
	24	0.14	0.070	0.24	0.36	0.94	1.1	0.20
	168/ 192*	0.047	0.017	0.036	0.035	0.27	0.22	0.033
	672	0.022	0.0089	0.0079	0.0088	0.054	0.049	0.012
<i>Mean</i>		0.032	0.014	0.023	0.029	0.15	0.15	0.024
<i>%WO<sub>Sr</sub></i>		3	5	2	8	10	11	4

201  
 202 The overall leaching behaviour as seen in **Figure 3** is comparable for all samples and comprises a  
 203 decreasing leaching rate with increasing leaching time. E.g. *LR<sub>Cs</sub>* for AAM\_1 is 49 mg/(m<sup>2</sup>.s) in the  
 204 first hour of leaching, decreases with a factor 10 for each following step (24 h, 7 d) and levels off in  
 205 the final interval (see **Table 3**). For both Cs<sup>+</sup> and Sr<sup>2+</sup>, the leach rate for all samples is highest in the  
 206 first hour of leaching. This behaviour is typical for materials with an initial surface wash-off, which is a  
 207 process that occurs often in this type of tank test for monolithic materials and comprises the fast  
 208 dissolution of soluble salts from the surface of the monolith [33]. In addition to surface wash-off,  
 209 diffusion of the element of interest through the sample and eventual depletion of the element from  
 210 the sample are important processes governing the leaching behaviour.

211 Diffusion-controlled release from a monolithic waste form is related to the surface area of the waste  
 212 form and the time of exposure [33]. In semi-dynamic tank leaching tests with a monolithic sample, a  
 213 one-dimensional semi-infinite diffusion model, based on Fick's second law, is often assumed [34,35].

214 In this model, mass transfer is assumed to take place in response to concentration gradients in the  
215 pore water solution of the structure [35]. When Fickian diffusion is considered as the dominant  
216 release mechanism, the mass release should be proportional to the square root of the release time  
217 ( $R \sim t^{0.5}$ ); this results in a straight line with a slope of 0.5 when the logarithm of the cumulative  
218 release is plotted against the logarithm of the release time [35]. Initial surface wash-off causes a  
219 higher release in the first stage of leaching, while depletion leads to a levelling-off of the cumulative  
220 release curve [33].

221 **Figure 4** shows the cumulative **caesium and strontium** release of a selected subset of samples (the  
222 remaining samples show similar behaviour) plotted against the release time on a double logarithmic  
223 scale. None of the samples closely follow the 0.5 slope. Since an initial wash-off and depletion of  $\text{Cs}^+$   
224 is clear from **Table 2** and **Table 3**, the results from the leaching test can be divided into the intervals  
225 [1 h ; 24 h] and [24 h ; 28 d] as shown in **Figure 4a** for  $\text{Cs}^+$  and **Figure 4b** for  $\text{Sr}^{2+}$ .

226 For **caesium**, it is clear from **Figure 4a** that the sample with limited wash-off (AAM\_1.1, as seen in  
227 **Table 3**) has a slope close to 0.5 in the interval [1 h ; 24 h] indicating possible diffusion-controlled  
228 release. AAM\_2 shows a slope of 0.28 in this first interval, indicating a significant wash-off (high  
229 concentration in the first hour of leaching).

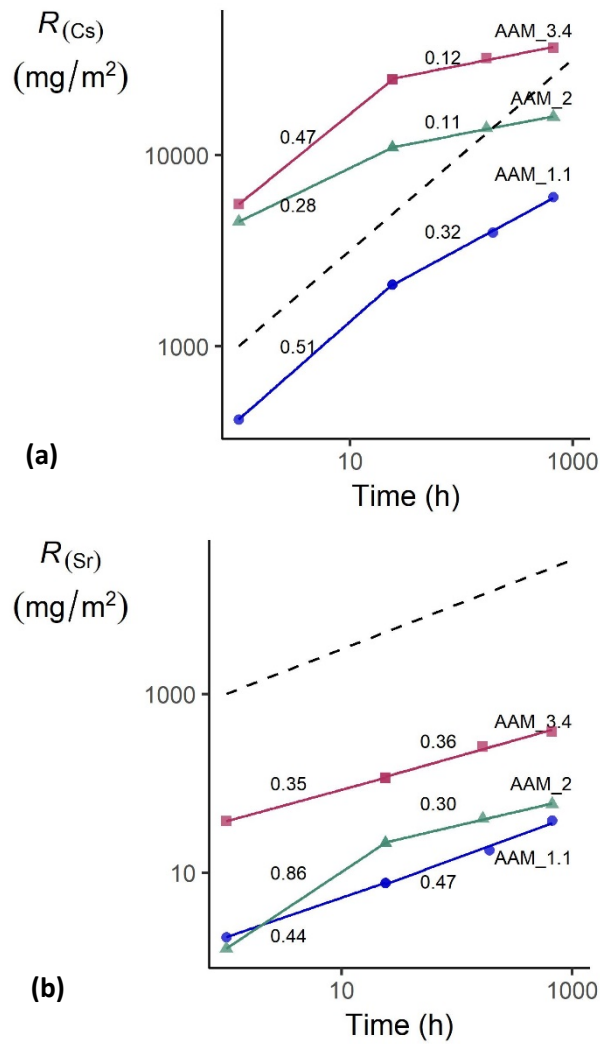
230 In the interval [24 h ; 28 d], the regression lines flatten for all samples (slope < 0.5) indicating signs of  
231 depletion. Since depletion is only assumed to occur when the total release is higher than 20 % [35],  
232 not all samples have actually been significantly depleted. **Table 2** shows that the release of  $\text{Cs}^+$  from  
233 the AAMs is between 46 and 7 %. The fact that depletion-like behaviour occurs even in samples with  
234 a low release indicates a possible distribution of the present  $\text{Cs}^+$  into an easily-leachable fraction and  
235 a strongly-bound fraction. The occurrence of the wash-off and the depletion effects can then be  
236 contributed to the easily-leachable fraction. The levelling-off of the regression curve could thus be  
237 caused by the depletion of the readily available  $\text{Cs}^+$ , while the remaining fraction is more strongly  
238 bound in the AAM structure. The leaching behaviour of  $\text{Cs}^+$  can thus be summarized as a combination

239 of initial wash-off, diffusion, and depletion of an easily-released fraction. The lower the Si/Al and  
240 Ca/(Si+Al) ratio, the smaller this easily-leachable fraction (as discussed further).

241 For **strontium**, the leaching behaviour in most samples does not seem to be dependent on the  
242 leaching interval as seen in **Figure 4b**. The overall slopes of the regression curves are smaller than  
243 0.5, indicating depletion. Since the total amount of leached  $\text{Sr}^{2+}$  is small for all samples (< 5 %, see  
244 **Table 2**), it seems reasonable that  $\text{Sr}^{2+}$  leaches only from the sample surface, slowly depleting while  
245 the bulk of the  $\text{Sr}^{2+}$  remains encapsulated in the sample, not available for leaching.

246 The amount of **sodium** leached does not correspond with the amount of  $\text{Cs}^+$  leached (see **Table 2**), as  
247 would be expected since  $\text{Cs}^+$  is known to act as a charge-balancing ion, replacing  $\text{Na}^+$  in the  
248 framework [13,15]. This indicates that  $\text{Cs}^+$  and  $\text{Na}^+$  immobilisation is not completely similar, and  
249 shows that  $\text{Cs}^+$  is retained better than  $\text{Na}^+$  (since  $\text{Na}^+$  release is higher and both were introduced as 1  
250 wt%). This is consistent with the findings of *Kuenzel et al. (2015)* [15], who reported that the reaction  
251 between  $\text{Cs}^+$  and  $\text{Al}(\text{OH})_4^-$  is favoured over that of  $\text{Na}^+$  because of the lower charge density of  $\text{Cs}^+$ . In  
252 addition, the difference in immobilisation between  $\text{Cs}^+$  and  $\text{Na}^+$  is dependent on the AAM  
253 composition, since from **Table 2** it can be seen that e.g. AAM\_2 releases the least  $\text{Na}^+$  (46 %) while  
254 releasing 20 %  $\text{Cs}^+$ ; in contrast, AAM\_1 leaches less  $\text{Cs}^+$  (14 %) and more  $\text{Na}^+$  (58 %). This could  
255 indicate a difference in hydrate phases formed depending on the AAM composition. The findings of  
256 *Kuenzel et al. (2015)* [15] were based on MK-AAMs, resulting in an amorphous sodium  
257 aluminosilicate hydrate (N-A-S-H) as the main binder phase.

258 A difference in the amount of N-A-S-H formed (as compared to calcium sodium aluminosilicate  
259 hydrate (C-(N)-A-S-H)) could be the cause of the difference in leaching behaviour of  $\text{Na}^+$  as compared  
260 to  $\text{Cs}^+$ . Based on the initial composition of the slags and the use of a NaOH activator, the AAMs are  
261 expected to consist mainly of C-(N)-A-S-H gel, N-A-S-H gel (due to high Al content), strätlingite, and  
262 some zeolitic phases [36–38]. For the low Si/Al samples AAM\_1 and AAM\_1.1, the ratio of leached  
263  $\text{Na}^+/\text{Cs}^+$  is much higher than for the high Si/Al samples (see **Table 2**).



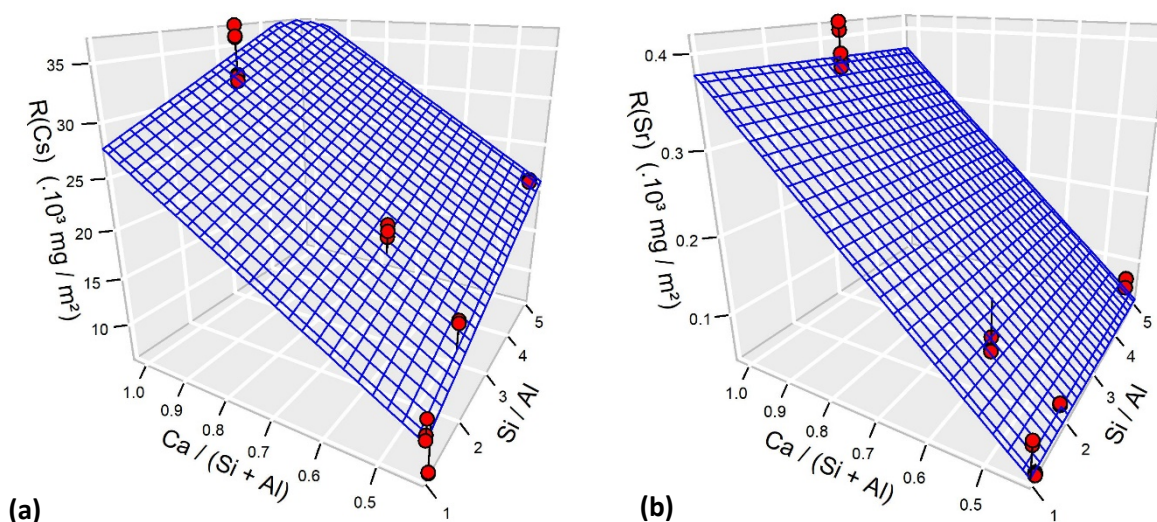
264

265 **Figure 4: (a)**  $R_{Cs}$ , dividing the leaching time into two intervals [1 h ; 24 h] and [24 h ; 28 d] and **(b)**  
 266  $R_{Sr}$ , dividing the leaching time into two intervals.  $R^2$ -values are all > 0.97 for **(a)** and **(b)**. The dashed  
 267 line represents the slope of 0.5 from a diffusion-based release. The slopes are indicated on the graph  
 268 next to the regression lines.

269 When linking the immobilisation capacity for  $Cs^+$  and  $Sr^{2+}$  with the precursor composition, an initial  
 270 Si/Al ratio of about 1.1 (**Table 2**) seems to be best. **Figure 5a** shows the cumulative 28-d release of  
 271  $Cs^+$  in function of the Si/Al and Ca/(Si+Al) ratios of the precursor slags. For the studied compositions,  
 272  $Cs^+$  is immobilised better in AAMs with lower Si/Al ratios and lower Ca/(Si+Al) ratios.



273 **Figure 5b** shows the cumulative 28-d release of  $\text{Sr}^{2+}$  in function of the Si/Al and Ca/(Si+Al) ratios of  
 274 the precursor slags. For the studied compositions, the immobilisation of  $\text{Sr}^{2+}$  is dependent on the  
 275 Ca/(Si+Al) ratio, but not on the Si/Al ratio. This indicates a competition between  $\text{Ca}^{2+}$  and  $\text{Sr}^{2+}$  for  
 276 incorporation into the AAM structure. The independence of strontium leaching to the Si/Al ratio is in  
 277 contrast with the results of the study of *Aly, et al.* (2008) [12], where  $\text{Sr}^{2+}$  release increased in  
 278 samples with an increasing Si/Al ratio from 1.5 to 4. This could be due to the fact that the samples  
 279 studied by *Aly, et al.* (2008) [12] were low in calcium, indicating the possible differences in leaching  
 280 behaviour in function of the type of AAMs.



281 **Figure 5:** The cumulative 28-d release of Cs<sup>+</sup> (a) and Sr<sup>2+</sup> (b) (10<sup>3</sup> mg/m<sup>2</sup>) in function of the Si/Al and  
 282 Ca/(Si+Al) ratios of the precursor slags. The regression planes are a result of multiple linear  
 283 regressions with R<sup>2</sup>-values > 0.93.

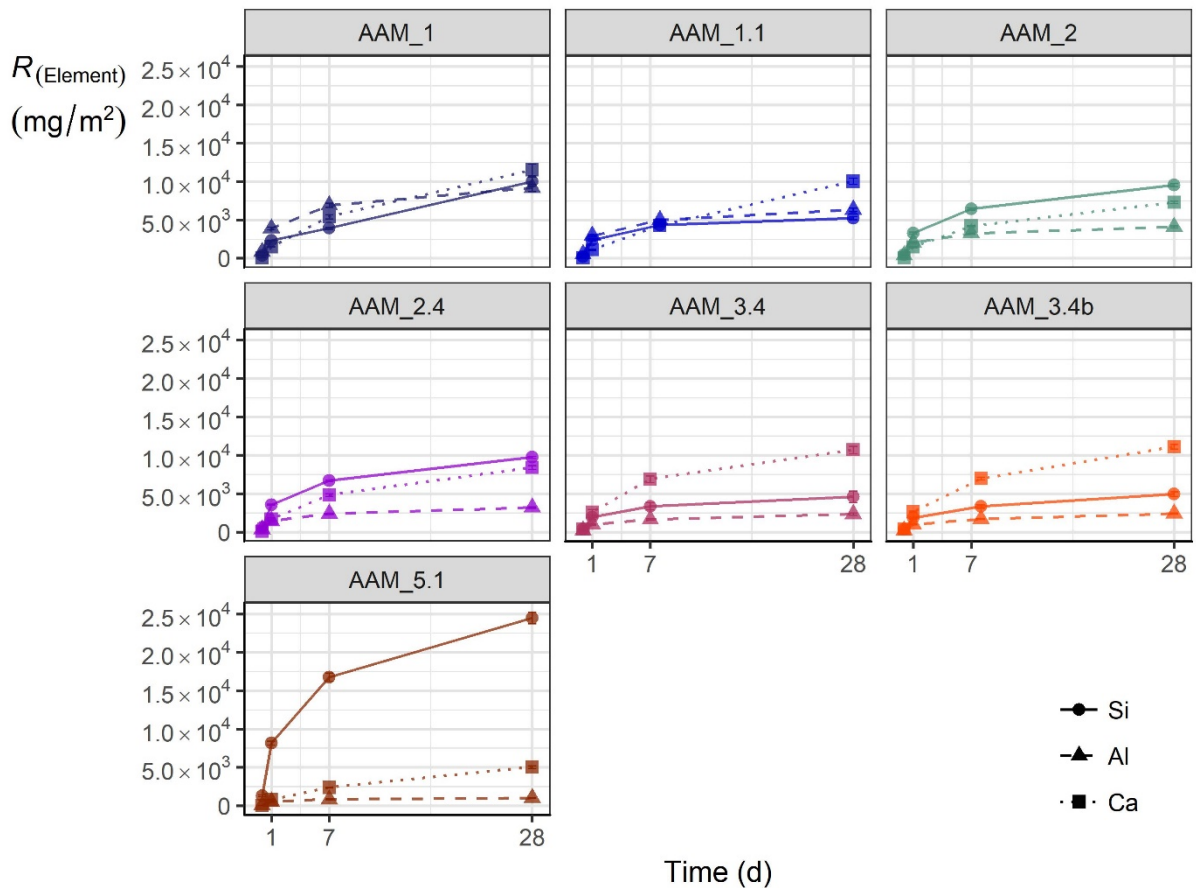
### 284 3.3 Release of structural elements

285 The Ca<sup>2+</sup> release of AAM\_1, AAM\_1.1, AAM\_3.4 and AAM\_3.4b are similar, while S\_1 and S\_1.1 have  
 286 a CaO content of only 30 % and S\_3.4 and S\_3.4b have an initial CaO content of 50 %. Also, the Ca<sup>2+</sup>  
 287 release decreases with increasing Si/Al ratio reaching a value of 7300 ± 200 mg/m<sup>2</sup> for AAM\_2 and  
 288 5000 ± 200 mg/m<sup>2</sup> for AAM\_5.1. This higher Ca<sup>2+</sup> release at lower Si/Al ratios explains why AAM\_1,  
 289 AAM\_1.1, AAM\_3.4 and AAM\_3.4b show a similar Ca<sup>2+</sup> release while having a lower calcium content.

290 This behaviour of calcium leaching could be an indication of less C-(N)-A-S-H formation at lower Si/Al  
291 ratios since the formation of this phase would better immobilise  $\text{Ca}^{2+}$  into the structure. An increased  
292 Al content (and thus lower Si/Al ratio) promotes the formation of N-A-S-H in addition to C-(N)-A-S-H,  
293 while an increased Ca content impedes the formation of N-A-S-H [38]. Higher Si/Al ratios will thus  
294 give rise to more C-(N)-A-S-H formation.

295 The highest **silicon** release is observed in AAM\_5.1 ( $\approx 24\,000\text{ mg/m}^2$ ), while AAM\_3.4, AAM\_3.4b,  
296 and AAM\_1.1 show the lowest silicon release ( $\approx 5000\text{ mg/m}^2$ ). AAM\_2.4, AAM\_2, and AAM\_1 all  
297 show a 28-d cumulative silicon release around  $10\,000\text{ mg/m}^2$ . The lower silicon leaching of AAM\_3.4  
298 and AAM\_3.4b as compared to AAM\_2.4, AAM\_2, and AAM\_1 (while having similar initial  $\text{SiO}_2$   
299 contents) indicates that a higher calcium content increases the immobilisation of silicon, which again  
300 indicates the formation of C-(N)-A-S-H.

301 Regarding **aluminium**, the release follows the Si/Al ratio, with AAM\_5.1 showing the lowest  
302 aluminium release and increasing with decreasing Si/Al. For AAM\_1, the amount of silicon and  
303 aluminium released is almost equal (AAM\_1:  $R_{\text{Si}} = 10000 \pm 600\text{ mg/m}^2$ ,  $R_{\text{Al}} = 9200 \pm 500\text{ mg/m}^2$ ),  
304 indicating congruent dissolution.



305

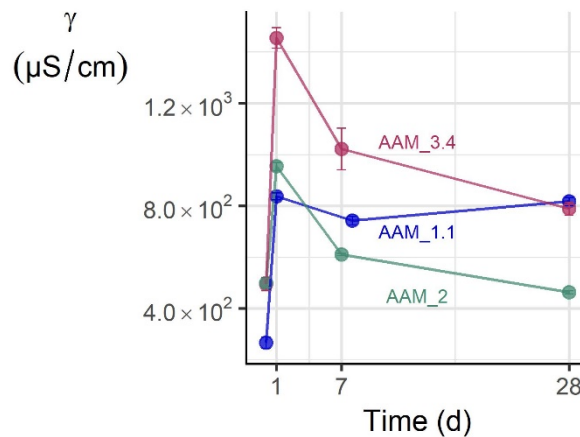
306 **Figure 6:** Cumulative release of silicon, aluminium and calcium during a 28-d leaching test at 90 °C.

307 *3.4 pH and conductivity*

308 The measured pH of the eluates was similar for all samples. After 1 h of leaching the average pH over  
 309 all samples was  $10.7 \pm 0.3$ . After 24 h, the pH of the eluates increased to  $11.2 \pm 0.3$ . After 28 d, the  
 310 pH-values were  $11.3 \pm 0.6$ . The conductivity of selected eluates is given in **Figure 7**.

311 AAM\_5.1, AAM\_3.4, AAM\_3.4b, AAM\_2.4 and AAM\_2 show a high peak in conductivity at 24 h (only  
 312 AAM\_2 and AAM\_3.4 shown in **Figure 7**), while decreasing at later sampling times. This high early  
 313 peak in ionic conductivity followed by a gradual decrease indicates a more profound early wash-off  
 314 and subsequent depletion, which is consistent with the results seen for  $\text{Cs}^+$  in **Figure 4a**. This effect is  
 315 not so pronounced for AAM\_1.1, which shows a slighter decrease in conductivity at the 7 d sampling  
 316 time. Regarding the validity of the experimental design, the duplicates AAM\_3.4 and AAM\_3.4b show

317 very similar results in all measured leaching aspects, confirming that the slag development, the AAM  
 318 development, and the leaching tests are very well reproducible.



319

320 **Figure 7:** Conductivity values (μS/cm) of AAM\_1.1, AAM\_2 and AAM\_3.4 at each sampling time.

321 *3.5 Effect of leaching temperature on immobilisation capacity*

322

323 **Table 4** and **Table 5** show that the leaching temperature has a profound effect on the release of all  
 324 constituents. However, this effect is not the same for all samples. AAM\_1 exhibits significantly less  
 325 release at 20 °C than at 90 °C for Cs<sup>+</sup>, Sr<sup>2+</sup> and Na<sup>+</sup>, while AAM\_5.1 exhibits less release for Sr<sup>2+</sup> and  
 326 Na<sup>+</sup> but not for Cs<sup>+</sup>. In contrast, AAM\_1.1 has a significantly higher release at 20 °C as compared to 90  
 327 °C for all constituents, while AAM\_2 has a higher release for Cs<sup>+</sup> and Na<sup>+</sup> at 20 °C and a similar release  
 328 for Sr<sup>2+</sup>. Although all samples were completely set after 28 days of curing, it appears that the high  
 329 temperature (90 °C) of the leaching environment influenced the curing of AAM\_1.1 and AAM\_2  
 330 which significantly improved their immobilisation potential. This does not seem to be the case for  
 331 AAM\_1 and AAM\_5.1.

332 **Table 4:** Slag Blaine values, % *release* and BET values for samples leached for 7 d at 20 °C. The  
 333 % *release* values are given as individual measurements since only one or two samples were tested  
 334 per composition.

Sample	Slag Blaine (m <sup>2</sup> /kg)			% release 7 d, 20 °C			BET (m <sup>2</sup> /g)		
				Cs <sup>+</sup>	Sr <sup>2+</sup>	Na <sup>+</sup>			
AAM_1	110	±	20	2.97; 3.06	0.13; 0.22	31.52; 31.77	10.7	±	0.1
AAM_1.1	200	±	20	11.22	4.02	60.21	14.8	±	0.1
AAM_2	140	±	10	26.56; 27.94	0.27; 0.49	41.29; 42.76	3.8	±	0.1
AAM_5.1	310	±	10	22.45; 22.71	0.20; 0.22	53.88; 55.21	37.5	±	0.1

335

336 **Table 5:** Percentages of Cs<sup>+</sup>, Sr<sup>2+</sup> and Na<sup>+</sup> released after 7 d leaching at 90 °C.

Sample	% release 7 d, 90 °C								
	Cs <sup>+</sup>			Sr <sup>2+</sup>			Na <sup>+</sup>		
AAM_1	10	±	1	0.48	±	0.05	46	±	2
AAM_1.1	5.1	±	0.2	0.23	±	0.03	41	±	1
AAM_2	17.5	±	0.3	0.51	±	0.2	36	±	1
AAM_5.1	24.2	±	0.7	0.49	±	0.06	62	±	2

337

338

### 339 3.6 Effect of specific surface area on immobilisation capacity

340 The BET specific surface area (before leaching) of the samples used for leaching at 20 °C is given in

341 **Table 4.** The BET specific surface area is lowest for AAM\_2, while AAM\_5.1 exhibits the highest BET

342 area. The specific surface areas of AAM\_1 and AAM\_1.1 are comparable. AAM\_2 releases more Cs<sup>+</sup>

343 and Sr<sup>2+</sup> than AAM\_5.1 at 20 °C, although having a much lower BET value. From the tested samples,

344 no clear correlation could be established between the BET values and the immobilisation capacities.

### 345 3.7 Effect of slag fineness on immobilisation capacity

346 The remainder of slag precursors S\_1 and S\_2 were further milled for an additional 30 s. The higher

347 Blaine values (HB) of these slags are given in **Table 6.** From these finer slags, additional samples of

348 composition AAM\_1 and AAM\_2 were prepared for leaching during 7 d at  $20 \pm 1$  °C. The percentages  
 349 of  $\text{Cs}^+$ ,  $\text{Sr}^{2+}$  and  $\text{Na}^+$  leached under these new leaching conditions are given in **Table 6**.

350 Increasing the slag fineness of S\_2 to a comparable value of that of S\_5.1 (see **Table 4**) reduces the  
 351  $\text{Cs}^+$  and  $\text{Sr}^{2+}$  release of AAM\_2 by a factor 2, increasing its immobilisation capacity beyond that of  
 352 AAM\_5.1. AAM\_1 shows the greatest immobilisation potential for all constituents at 20 °C, despite  
 353 having the smallest Blaine specific surface area of the slag. Increasing the slag fineness of S\_1 and  
 354 S\_2 demonstrates its significant effect on the immobilisation potential. The increased Blaine value of  
 355  $220 \text{ m}^2/\text{kg}$  for S\_1 (which is now comparable to that of S\_1.1) further increases the immobilisation  
 356 potential for all constituents. The same effect is observed for AAM\_2. Increasing the slag fineness  
 357 leads to a larger fraction of small slag particles that can be readily dissolved to form hydrate phases.  
 358 This, in turn, raises the need for more charge-balancing ions, thus increasing the incorporation  
 359 potential.

360 The results of the effect of leaching temperature, and the differences in specific surface area and slag  
 361 fineness support the earlier established relationship between the immobilisation potential and  
 362 design parameters Si/Al and Ca/(Si+Al). Leaching at 20 °C strengthens the conclusion that low Si/Al  
 363 and Ca/(Si+Al) ratios provide a higher immobilisation potential since AAM\_1 now exhibits the best  
 364 immobilisation potential (see **Table 5** and **Table 6**). Under the experimental conditions, a Si/Al ratio  
 365 of 1 thus seems optimal for immobilising  $\text{Cs}^+$  and  $\text{Sr}^{2+}$ .

366

367 **Table 6:** Higher Blaine values (HB) after additional milling and % *release* after 7 d leaching at 20 °C  
 368 of AAM\_1 and AAM\_2 prepared with HB-slag.

Sample	Slag Blaine HB ( $\text{m}^2/\text{kg}$ )	% <i>release</i> 7 d, 20 °C		
		$\text{Cs}^+$	$\text{Sr}^{2+}$	$\text{Na}^+$
AAM_1	220 ± 10	2.38	0.05	22.03
AAM_2	380 ± 10	12.79	0.18	31.48

369

370

#### 371 **4 Conclusion**

372 The effect of AAM composition regarding Si/Al and Ca/(Si+Al) ratios on the immobilisation capacity of  
373 introduced Cs<sup>+</sup> and Sr<sup>2+</sup> is discussed. Stoichiometrically controlled slags were designed from analytical  
374 grade chemicals to serve as precursors for monolithic AAM samples for immobilisation purposes.

375 Under the given experimental conditions, the following conclusions are made:

- 376 a) Very effective immobilisation of Cs<sup>+</sup> and Sr<sup>2+</sup> was achieved by use of low-alkaline AAMs. An  
377 immobilisation potential of up to 97.6 % and 99.9 % of introduced Cs<sup>+</sup> and Sr<sup>2+</sup> respectively was  
378 achieved for composition AAM\_1, after 7 days of leaching at 20 °C.
- 379 b) The leaching behaviour of Cs<sup>+</sup> from the AAMs consists of a combination of initial wash-off,  
380 diffusion and depletion of an easily-leachable fraction. Sr<sup>2+</sup> leaching appears to be limited to a  
381 small fraction present on or near the surface, showing less wash-off and exhibiting slow  
382 depletion.
- 383 c) Cs<sup>+</sup> immobilisation is dependent on the Si/Al and Ca/(Si+Al) ratios of the precursor while Sr<sup>2+</sup>  
384 immobilisation is only dependent on the Ca/(Si+Al) ratio. Better immobilisation is achieved at  
385 lower ratios, independent of the observed differences in precursor fineness or AAM specific  
386 surface area.
- 387 d) Lowering the leaching temperature from 90 °C to 20 °C has a varying effect on the immobilisation  
388 capacity of different compositions. This highlights the importance of being aware that leaching  
389 conditions affect obtained results, especially when comparing compositions. Leaching at higher  
390 temperature affects the curing of the AAMs, which can lead to misinterpretations of leaching  
391 results when comparing immobilisation capacities of different compositions.

392 In general, the developed AAMs show very effective Cs<sup>+</sup> and Sr<sup>2+</sup> immobilisation which is very  
393 promising for the use of AAMs for waste immobilisation purposes. This study offers a deeper

394 understanding of the immobilisation mechanism of AAMs, which could encourage further research in  
395 finding better alternatives for RAW immobilisation, and, in turn, encourage its large-scale  
396 application.

### 397 **Acknowledgements**

398 The authors thank Joris Van Dyck (KU Leuven, Department of Materials Engineering) for his  
399 assistance in developing the slag precursors, Elsy Thijssen and Martine Vanhamel (Hasselt University,  
400 CMK, Research Group of Applied and Analytical Chemistry) for their help regarding ICP-OES and ICP-  
401 MS measurements, and Bart Ruttens (IMEC, Division IMOMECE) for the XRD measurements.

### 402 **Data availability**

403 The raw/processed data required to reproduce these findings cannot be shared at this time as the  
404 data also forms part of an ongoing study.

### 405 **References**

- 406 [1] P. Krivenko, Why alkaline activation - 60 years of the theory and practice of alkali-activated  
407 materials, *J. Ceram. Sci. Technol.* 8 (2017) 323–333. doi:10.4416/JCST2017-00042.
- 408 [2] J.L. Provis, Introduction and scope, in: *Alkali Act. Mater. State-of-the-Art Report*, RILEM TC  
409 224-AAM, 2014: pp. 1–9.
- 410 [3] W. Xuequan, Y. Sheng, S. Xiaodong, T. Mingshu, Y. Liji, Alkali-activated slag cement based  
411 radioactive waste forms, *Cem. Concr. Res.* 21 (1991) 16–20. doi:10.1016/0008-  
412 8846(91)90026-E.
- 413 [4] S. Xiaodong, Y. Sheng, W. Xuequan, T. Mingshu, Y. Liji, Immobilization of simulated high level  
414 wastes into AASC waste form, *Cem. Concr. Res.* 24 (1994) 133–138. doi:10.1016/0008-  
415 8846(94)90094-9.
- 416 [5] M.Y. Khalil, E. Merz, Immobilization of intermediate-level wastes in geopolymers, *J. Nucl.*  
417 *Mater.* 211 (1994) 141–148. doi:10.1016/0022-3115(94)90364-6.
- 418 [6] G. Qian, D.D. Sun, J.H. Tay, New aluminium-rich alkali slag matrix with clay minerals for  
419 immobilizing simulated radioactive Sr and Cs waste, *J. Nucl. Mater.* 299 (2001) 199–204.  
420 doi:10.1016/S0022-3115(01)00700-0.
- 421 [7] Q. Guangren, L. Yuxiang, Y. Facheng, S. Rongming, Improvement of metakaolin on radioactive  
422 Sr and Cs immobilization of alkali-activated slag matrix, *J. Hazard. Mater.* 92 (2002) 289–300.



- 423 doi:10.1016/S0304-3894(02)00022-5.
- 424 [8] A. Fernandez-Jimenez, D.E. MacPhee, E.E. Lachowski, A. Palomo, Immobilization of cesium in  
425 alkaline activated fly ash matrix, *J. Nucl. Mater.* 346 (2005) 185–193.  
426 doi:10.1016/j.jnucmat.2005.06.006.
- 427 [9] C. Shi, a. Fernández-Jiménez, Stabilization/solidification of hazardous and radioactive wastes  
428 with alkali-activated cements, *J. Hazard. Mater.* 137 (2006) 1656–1663.  
429 doi:10.1016/j.jhazmat.2006.05.008.
- 430 [10] S. Goni, A. Guerrero, M.P. Lorenzo, Efficiency of fly ash belite cement and zeolite matrices for  
431 immobilizing cesium, *J. Hazard. Mater.* 137 (2006) 1608–1617.  
432 doi:10.1016/j.jhazmat.2006.04.059.
- 433 [11] M.G. Blackford, J. V. Hanna, K.J. Pike, E.R. Vance, D.S. Perera, Transmission electron  
434 microscopy and nuclear magnetic resonance studies of geopolymers for radioactive waste  
435 immobilization, *J. Am. Ceram. Soc.* 90 (2007) 1193–1199. doi:10.1111/j.1551-  
436 2916.2007.01532.x.
- 437 [12] Z. Aly, E.R. Vance, D.S. Perera, J. V. Hanna, C.S. Griffith, J. Davis, D. Durce, Aqueous leachability  
438 of metakaolin-based geopolymers with molar ratios of Si/Al = 1.5-4, *J. Nucl. Mater.* 378 (2008)  
439 172–179. doi:10.1016/j.jnucmat.2008.06.015.
- 440 [13] J.L. Provis, P.A. Walls, J.S.J. van Deventer, Geopolymerisation kinetics. 3. Effects of Cs and Sr  
441 salts, *Chem. Eng. Sci.* 63 (2008) 4480–4489. doi:10.1016/j.ces.2008.06.008.
- 442 [14] Q. Li, Z. Sun, D. Tao, Y. Xu, P. Li, H. Cui, J. Zhai, Immobilization of simulated radionuclide  
443  $^{133}\text{Cs}^+$  by fly ash-based geopolymer, *J. Hazard. Mater.* 262 (2013) 325–331.  
444 doi:10.1016/j.jhazmat.2013.08.049.
- 445 [15] C. Kuenzel, J.F. Cisneros, T.P. Neville, L. Vandeperre, S.J.R. Simons, J. Bensted, C.R.  
446 Cheeseman, Encapsulation of Cs/Sr contaminated clinoptilolite geopolymers produced from  
447 metakaolin, *J. Nucl. Mater.* 466 (2015) 94–99.
- 448 [16] J.G. Jang, S.M. Park, H.K. Lee, Physical barrier effect of geopolymeric waste form on diffusivity  
449 of cesium and strontium, *J. Hazard. Mater.* 318 (2016) 339–346.  
450 doi:10.1016/j.jhazmat.2016.07.003.
- 451 [17] X. Peng, Y. Xu, Z. Xu, D. Wu, D. Li, Effect of simulated radionuclide strontium on  
452 geopolymerization process, *Procedia Environ. Sci.* 31 (2016) 325–329.  
453 doi:10.1016/j.proenv.2016.02.043.
- 454 [18] Z. Li, T. Ohnuki, K. Ikeda, Development of paper sludge ash-based geopolymer and application  
455 to treatment of hazardous water contaminated with radioisotopes, *Materials (Basel)*. 9 (2016)  
456 633. doi:10.3390/ma9080633.
- 457 [19] Z. Xu, Z. Jiang, D. Wu, X. Peng, Y. Xu, N. Li, Y. Qi, P. Li, Immobilization of strontium-loaded  
458 zeolite A by metakaolin based-geopolymer, *Ceram. Int.* 43 (2017) 4434–4439.  
459 doi:10.1016/j.ceramint.2016.12.092.
- 460 [20] J. Jang, S. Park, H. Lee, Cesium and strontium retentions governed by aluminosilicate gel in  
461 alkali-activated cements, *Materials (Basel)*. 10 (2017). doi:10.3390/ma10040447.
- 462 [21] K. Shiota, T. Nakamura, M. Takaoka, S.F. Aminuddin, K. Oshita, T. Fujimori, Stabilization of  
463 cesium in alkali-activated municipal solid waste incineration fly ash and a pyrophyllite-based  
464 system, *Chemosphere*. 187 (2017) 188–195. doi:10.1016/j.chemosphere.2017.08.114.
- 465 [22] K. Shiota, T. Nakamura, M. Takaoka, K. Nitta, K. Oshita, T. Fujimori, T. Ina, Chemical kinetics of

- 466 Cs species in an alkali-activated municipal solid waste incineration fly ash and pyrophyllite-  
 467 based system using Cs K-edge in situ X-ray absorption fine structure analysis, *Spectrochim.*  
 468 *Acta - Part B At. Spectrosc.* 131 (2017) 32–39. doi:10.1016/j.sab.2017.03.003.
- 469 [23] J. Zhang, J.L. Provis, D. Feng, J.S.J. van Deventer, Geopolymers for immobilization of Cr<sup>6+</sup>,  
 470 Cd<sup>2+</sup>, and Pb<sup>2+</sup>, *J. Hazard. Mater.* 157 (2008) 587–598. doi:10.1016/j.jhazmat.2008.01.053.
- 471 [24] T. Hanzlicek, M. Steinerova, P. Straka, Radioactive metal isotopes stabilized in a geopolymer  
 472 matrix: Determination of a leaching extract by a radiotracer method, *J. Am. Ceram. Soc.* 89  
 473 (2006) 3541–3543. doi:10.1111/j.1551-2916.2006.01024.x.
- 474 [25] P. Lichvar, M. Rozloznik, S. Sekely, Behaviour of aluminosilicate inorganic matrix SIAL<sup>®</sup> during  
 475 and after solidification of radioactive sludge and radioactive spent resins and their mixtures,  
 476 *Proc. IAEA Meet. Kalpakkam, India.* (2010).
- 477 [26] M.R. El-Naggar, Applicability of alkali activated slag-seeded Egyptian Sinai kaolin for the  
 478 immobilization of <sup>60</sup>Co radionuclide, *J. Nucl. Mater.* 447 (2014) 15–21.  
 479 doi:10.1016/j.jnucmat.2013.12.020.
- 480 [27] International Atomic Energy Agency, The behaviours of cementitious materials in long term  
 481 storage and disposal of radioactive waste : results of a coordinated research project, Vienna,  
 482 2013.
- 483 [28] European Committee for Standardization, EN 196-6:2010 - Methods of testing cement - Part  
 484 6: Determination of fineness, 2010.
- 485 [29] N. Vandevenne, R.I. Iacobescu, Y. Pontikes, R. Carleer, E. Thijssen, K. Gijbels, S. Schreurs, W.  
 486 Schroevers, Incorporating Cs and Sr into blast furnace slag inorganic polymers and their effect  
 487 on matrix properties, *J. Nucl. Mater.* 503 (2018) 1–12. doi:10.1016/j.jnucmat.2018.02.023.
- 488 [30] N. Vandevenne, R.I. Iacobescu, Y. Pontikes, K. Gijbels, S. Schreurs, W. Schroevers, The effect of  
 489 Cs and Sr on the mechanical properties of blast furnace slag inorganic polymer for radioactive  
 490 waste immobilisation, in: *5th Int. Slag Valoris. Symp.*, 2017: pp. 401–404.
- 491 [31] ASTM, C 1220 - 98 Standard test method for static leaching of monolithic waste forms for  
 492 disposal of radioactive waste, (1998).
- 493 [32] European Committee for Standardization, CEN/TS 15863:2015: Characterisation of waste -  
 494 Leaching behaviour test for basic characterisation - Dynamic monolithic leaching test with  
 495 periodic leachant renewal, under fixed test conditions, 2015.
- 496 [33] H.A. van der Sloot, J.J. Dijkstra, Development of horizontally standardized leaching tests for  
 497 construction materials: a material based or release based approach?, (2004) 56.
- 498 [34] A.C. Garrabrants, D.S. Kosson, H.A. Van Der Sloot, F. Sanchez, O. Hjelmars., Background  
 499 information for the Leaching Environmental Assessment Framework (LEAF) test methods, U.S.  
 500 *Environ. Prot. Agency, Washington, DC.*, (2011).
- 501 [35] D.S. Kosson, H.A. van der Sloot, F. Sanchez, A.C. Garrabrants, An integrated framework for  
 502 evaluating leaching in waste management and utilization of secondary materials, *Environ.*  
 503 *Eng. Sci.* 19 (2002) 159–204. doi:10.1089/109287502760079188.
- 504 [36] R.J. Myers, S.A. Bernal, J.L. Provis, A thermodynamic model for C-(N)-A-S-H gel: CNASH-ss.  
 505 Derivation and validation, *Cem. Concr. Res.* 66 (2014) 27–47.  
 506 doi:10.1016/j.cemconres.2014.07.005.
- 507 [37] R.J. Myers, B. Lothenbach, S.A. Bernal, J.L. Provis, Thermodynamic modelling of alkali-  
 508 activated slag cements, *Appl. Geochemistry.* 61 (2015) 233–247.

509 doi:10.1016/j.apgeochem.2015.06.006.

510 [38] B. Walkley, R. San Nicolas, M.A. Sani, G.J. Rees, J. V. Hanna, J.S.J. van Deventer, J.L. Provis,  
511 Phase evolution of C-(N)-A-S-H/N-A-S-H gel blends investigated via alkali-activation of  
512 synthetic calcium aluminosilicate precursors, *Cem. Concr. Res.* 89 (2016) 120–135.  
513 doi:10.1016/j.cemconres.2016.08.010.

514